PCCP

Influence of Uranyl Complexation on the Reaction Kinetics of the Dodecane Radical Cation with Used Nuclear Fuel Extraction Ligands (TBP, DEHBA, and DEHiBA)

Journal:	*Physical Chemistry Chemical Physics*
Manuscript ID	CP-ART-08-2021-003797.R1
Article Type:	Paper
Date Submitted by the Author:	13-Oct-2021
Complete List of Authors:	Celis-Barros, Cristian; Florida State University, Chemistry and Biochemistry Pilgrim, Corey; Idaho National Laboratory, Cook, Andrew; Brookhaven National Laboratory, Chemistry Department Mezyk, Stephen; California State University at Long Beach, Chemistry and Biochemistry Grimes, Travis; Idaho National Laboratory, Aqueous Separations and Radiochemistry Horne, Gregory; Idaho National Laboratory, Center for Radiation Chemistry Research

ARTICLE

Influence of Uranyl Complexation on the Reaction Kinetics of the Dodecane Radical Cation with Used Nuclear Fuel Extraction Ligands (TBP, DEHBA, and DEH*i*BA)

Received 18th August 2021,
Accepted 00th September 2021

DOI: 10.1039/x0xx00000x

Cristian Celis Barros,[a]*Corey D. Pilgrim,[b] Andrew R. Cook,[c] Stephen P. Mezyk,[d] Travis S. Grimes,[b] and Gregory P. Horne[b]*

Specialized extractant ligands – such as tri-butyl phosphate (TBP), *N*,*N*-di-(2-ethylhexyl)butyramide (DEHBA), and *N*,*N*-di-2-ethylhexylisobutryamide (DEH*i*BA) – have been developed for the recovery of uranium from used nuclear fuel by reprocessing solvent extraction technologies. These ligands must function in the presence of an intense multi-component radiation field, and thus it is critical that their radiolytic behaviour be thoroughly evaluated. This is especially true for their metal complexes, where there is negligible information on the influence of complexation on radiolytic reactivity, despite the prevalence of metal complexes in used nuclear fuel reprocessing solvent systems. Here we present a kinetic investigation into the effect of uranyl (UO_2^{2+}) complexation on the reaction kinetics of the dodecane radical cation ($RH^{\bullet+}$) with TBP, DEHBA, and DEH*i*BA. Complexation had negligible effect on the reaction of $RH^{\bullet+}$ with TBP, for which a second-order rate coefficient (k) of $(1.3 \pm 0.1) \times 10^{10}$ M^{-1} s^{-1} was measured. For DEHBA and DEH*i*BA, UO_2^{2+} complexation afforded an increase in their respective rate coefficients: $k(RH^{\bullet+} + [UO_2(NO_3)_2(DEHBA)_2]) = (2.5 \pm 0.1) \times 10^{10}$ M^{-1} s^{-1} and $k(RH^{\bullet+} + [UO_2(NO_3)_2(DEHiBA)_2]) = (1.6 \pm 0.1) \times 10^{10}$ M^{-1} s^{-1}. This enhancement with complexation is indicative of an alternative $RH^{\bullet+}$ reaction pathway, which is more readily accessible for $[UO_2(NO_3)_2(DEHBA)_2]$ as it exhibited a much larger kinetic enhancement than $[UO_2(NO_3)_2(DEHiBA)_2]$, 2.6× *vs.* 1.4×, respectively. Complementary quantum mechanical calculations suggests that the difference in reaction kinetic enhancement between TBP and DEHBA/DEH*i*BA is attributed to a combination of reaction pathway (electron/hole transfer *vs.* proton transfer) energetics and electron density distribution, wherein attendant nitrate counter anions effectively 'shield' TBP from $RH^{\bullet+}$ electron transfer processes.

Introduction

Reprocessing used nuclear fuel (UNF) for the recovery of unspent fissile material (e.g., uranium-235 and plutonium-239) offers several potential advantages, including but not limited to: energy security through a closed nuclear fuel cycle; reduced dependence on front-end nuclear fuel-cycle activities, e.g., uranium mining and conversion; and a significant reduction in the long-term radiotoxic burden on nuclear waste geological repositories, from ~300,00 years to ~400 years.[1] UNF reprocessing has been successfully performed for decades by solvent extraction technologies, typically by some variant of the *Plutonium Uranium Reduction Extraction* (PUREX) process. [2,3]

The overall strategy of such processes is to extract uranium and plutonium from a concentrated nitric acid (HNO_3) aqueous phase in which the UNF has been dissolved. Separation of these metals is achieved using specialized ligands, such as tributyl phosphate (TBP, **Figure 1A**), to induce extraction into the organic phase. The partitioned uranium/plutonium ligand complexes are then sequentially recovered into fresh aqueous HNO_3 solution streams, free of other fission products. These reprocessing stages are performed in the presence of an intense multi-component radiation field emanating from the dissolved radioisotopic content of the UNF. Radiolysis of both the aqueous (H_2O, NO_3^-, and HNO_3) and organic solvent (RH) phases liberates a suite of reactive species, generalized by **Equations (1)** to **(3)**.[4-6] This indirect radiolysis is then capable of propagating degradation to the extraction ligand.

$$H_2O \rightsquigarrow e_{aq}^-, H^\bullet, {}^\bullet OH, H_2O_2, H_2, H_{aq}^+ \quad (1)$$

$$NO_3^-/HNO_3 \rightsquigarrow e_{aq}^-, NO_3^\bullet, NO_2^-/HNO_2, {}^\bullet O^\bullet \quad (2)$$

$$RH \rightsquigarrow e^-, H^\bullet, RH^{\bullet+}, R^\bullet. \quad (3)$$

Furthermore, for reprocessing solvent system formulations that employ large concentrations of extraction ligand (e.g., 30 vol.% TBP in the PUREX process), the ligand's electron density is sufficiently high for it to undergo direct radiolysis, i.e., the direct deposition of radiation energy into the ligand itself, **Equation (4)**:

[a] *Department of Chemistry and Biochemistry, Florida State University, Tallahassee, FL 32306, USA.*
[b] *Center for Radiation Chemistry Research, Idaho National Laboratory, Idaho Falls, ID, P.O. Box 1625, 83415, USA*
[c] *Department of Chemistry, Brookhaven National Laboratory, Upton, New York, 11973, USA.*
[d] *Department of Chemistry and Biochemistry, California State University Long Beach, 1250 Bellflower Boulevard, Long Beach California, 90840-9507, USA.*
E-mail: ccelisbarros@fsu.edu and gregory.p.horne@inl.gov
† Electronic Supplementary Information (ESI) available: additional computational figures and tables. See DOI: 10.1039/x0xx00000x

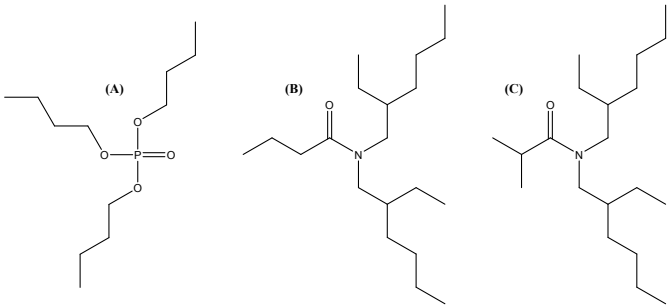

Fig. 1. Molecular structures of tri-butyl phosphate (TBP, **A**), *N*,*N*-di-(2-ethylhexyl)butyramide (DEHBA, **B**), and *N*,*N*-di-2-ethylhexylisobutryamide (DEH*i*BA, **C**).

ligand ⇝ degradation products. (4)

Both direct and indirect ligand radiolysis deplete the available concentration of extractant, and yield many degradation products which have the potential to interfere with complexation and negatively alter the physical and chemical properties of the solvent extraction system. These effects can be detrimental to process performance and solvent recyclability. Consequently, extraction ligands must not only be highly specific for their elemental target but also exhibit sufficient radiolytic integrity to ensure viable process performance. Therefore, thoroughly understanding this radiolytic behaviour is critical for solvent extraction technology.

Although TBP is the current industrial standard for reprocessing technology, there is incentive for its replacement by alternative ligands that yield less problematic degradation products from radiolysis,[7] and provide additional benefits such as tuneable selectivity (e.g., a preference for uranium over plutonium) and/or adherence to the CHON (composed of only Carbon, Hydrogen, Oxygen, and Nitrogen) principle for simplification of waste treatment for used solvents.[8,9] One such class of alternative ligands are the N,N-dialkyl monoamides,[10,11] in which *N*,*N*-di-(2-ethylhexyl)butyramide (DEHBA, **Figure 1B**) and its isomer *N*,*N*-di-2-ethylhexylisobutryamide (DEH*i*BA, **Figure 1C**) have been proposed as direct replacements for TBP. The utilization of one isomer over the other would be dictated by the type of closed fuel cycle adopted, as DEHBA facilitates efficient co-extraction of uranium and plutonium, while DEH*i*BA enables the selective extraction of uranium only.[12] Both of these monoamide ligands exhibit greater radiolytic stability than TBP, as demonstrated by their respective organic-only gamma radiolytic degradation yields (*G*-values): *G*(DEHBA)= -0.31 μmol J^{-1},[13] *G*(DEH*i*BA) = -0.30 μmol J^{-1},[14] and *G*(TBP) = -0.37 μmol J^{-1}.[14,15] However, the radiation chemistry of all three ligands has only been extensively evaluated in the absence of metal ions,[7,13-22] which is unrepresentative of reprocessing conditions wherein all three form at least bis-chelated nitrate (NO_3^-) complexes with the uranyl cation (UO_2^{2+}) and two NO_3^- counter-anions, ($[UO_2(NO_3)_2(L)_2]$.[23-26] Metal ion complexation can alter the radiolytic behaviour of a given ligand by facilitating alternative reaction pathways,[27] for example, a radical formed on a coordinated ligand ($L^\bullet$) can undergo electron transfer with the complexed metal ion ($[M(NO_3)_2(L)_2]$) as demonstrated in **Equations (5)** and **(6)** for an electron-transfer oxidation by the dodecane radical cation ($RH^{\bullet+}$):

$$[M(NO_3)_2(L)_2] + RH^{\bullet+} \rightarrow [M(NO_3)_2(L)(L^\bullet)]^+ + RH, \quad (5)$$

$$[M(NO_3)_2(L)(L^\bullet)]^+ \rightarrow [M^+(NO_3)_2(L)_2]. \quad (6)$$

This may regenerate the ligand, instigate ligand fragmentation, and/or destabilize the metal ion complex through generation of non-preferential metal orbital geometries.

The importance of this oversight in evaluating radiolytic robustness under envisioned reprocessing conditions was recently demonstrated for two ligands proposed for the separation of the trivalent actinides (An^{3+}) from the trivalent lanthanides (Ln^{3+}), hexa-*n*-octylnitrilo-triacetamide (HONTA)[28] and 2-ethylhexylphosphonic acid mono-2-ethylhexyl ester (HEH[EHP]).[29] Both ligands exhibited large changes (up to orders of magnitude) in radiation chemical kinetics upon metal ion complexation for their reaction with $RH^{\bullet+}$. The significant increase in reactivity between *f*-element complexed HONTA and HEH[EHP] with $RH^{\bullet+}$ suggested that their reported steady-state radiolytic robustness in the absence of metal ions may be significantly overestimated under process conditions.[30,31] This was found to be the case for HEH[EHP] gamma irradiated in the presence of its lanthanum (La^{3+}) complexes ($[La((HEH[EHP])_2)_3]$), wherein the overall rate of HEH[EHP] radiolysis increased by up to 40% within 1 MGy of absorbed dose.[29] Consequently, the influence of complexation on the radiolytic behaviour of TBP, DEHBA, and DEH*i*BA must be quantitatively evaluated to ascertain whether complexation increases the susceptibility of these ligands to radiolysis, especially as $RH^{\bullet+}$ is thought to play a significant role in inducing indirect radiolysis of reprocessing ligands.[32-36] Further, as the extent of metal loading for TBP/DEHBA/DEH*i*BA based solvent systems is of the order of molar – and not millimolar as is for ligands designed for the separation of An^{3+} from Ln^{3+} – such a kinetic effect is expected to be considerably more pronounced.

To evaluate the influence of metal complexation and determine whether a precedence exists for changes in steady-state irradiation behaviour for TBP, DEHBA, and DEH*i*BA, a combination of pulsed electron kinetic measurements irradiations and electronic structure calculations were employed to investigate the effect of uranyl (UO_2^{2+}) complexation on their $RH^{\bullet+}$ reaction kinetics.

Methodology

The uranium solutions employed in this work were radioactive. Handling was performed in dedicated radiological and nuclear facilities using well established radiological safety protocols.

Materials

Uranyl nitrate crystals ($UO_2(NO_3)_2.6H_2O$), from on-hand stock at the Idaho National Laboratory's (INL) Radiochemistry Laboratory (RCL), were dissolved in 3.97 M HNO_3 – standardized by titration – to prepare the uranium stock solution used in all subsequent manipulations. TBP (≥99.0%), n-dodecane (≥99% anhydrous), HNO_3 (≥99.999% trace metals basis), dichloromethane (DCM, ≥99.8%), and potassium thiocyanate (KSCN, ≥99.0% ACS Reagent Grade) were sourced from MilliporeSigma (Burlington, MA, USA). DEHBA (99%) and

DEH*i*BA (99%) were obtained from Technocomm Ltd. (Wellbrae, Scotland, UK). All chemicals were used as received without further purification. Ultra-pure water (> 18.2 MΩ cm^{-1}) was used in the preparation of all aqueous solutions.

Uranium extraction conditions were determined by using previously published uranium distribution ratios (DM = $[M]_{org}/[M]_{aq}$) for TBP,[37] DEHBA,[12] and DEH*i*BA[12] dissolved in *n*-dodecane. Extractions involved contacting 1.1 M ligand in 0.5 M DCM/*n*-dodecane solution – that had been pre-equilibrated three times with 3.97 M HNO_3 – with 0.21 M uranium in 3.97 M HNO_3 solution in a 1:1 organic-to-aqueous volume ratio for 1 minute using a vortex mixer. DCM was added to the *n*-dodecane solvent as an electron scavenger to extend the lifetime of $RH^{\bullet+}$ and inhibit competing reaction kinetics. The uranium loaded phases were left to settle overnight, and after separation were subsequently diluted with 0.5 M DCM/*n*-dodecane solution to attain a series of uranium-ligand complex concentrations with a fixed complexed to non-complexed (free) ratio. Complementary free ligand-only samples were also prepared for comparison. Diluted ligand and uranium-ligand solutions were then transferred to screw-cap, semi-micro, 10 mm pathlength Suprasil cuvettes for irradiation.

The remaining uranium loaded ligand stock solutions were used to determine the post-contact concentration of uranium by liquid scintillation counting (LSC). A 300 µL sample of each phase was introduced to 10 mL of scintillation cocktail (Optima Gold) and analysed by scintillation counting, using a PerkinElmer Tri-Carb 3180TR/SL Low Activity LSC, to determine the ratio of uranium activity in each phase, allowing calculation of D_M and ultimately the concentration of uranium in the organic phase of the stock solutions: 0.197 M in TBP, 0.175 M in DEHBA, and 0.144 M in DEH*i*BA.

Time-Resolved Pulsed Electron Irradiations

Dodecane radical cation reaction kinetics were measured for UO_2^{2+} loaded TBP, DEHBA, and DEH*i*BA in 0.5 M DCM/*n*-dodecane solutions using the Brookhaven National Laboratory (BNL) Laser Electron Accelerator Facility (LEAF).[38] An FND-100Q silicon photodiode (EG&G), LeCroy (Chestnut Ridge, NY, USA) WaveRunner 66Zi transient digitizer (600MHz, 12 bit resolution), and optical interference filters (10 nm bandpass) – for wavelength selection of the analysing light – were employed for direct measurement of $RH^{\bullet+}$ decay kinetics at 800 nm over 200 ns.[39,40]

Second-order rate coefficients (*k*) were subsequently determined by pseudo-first-order double-exponential fits to the $RH^{\bullet+}$ decay traces, corrected for free ligand and corresponding UO_2^{2+} complex ($[UO_2(NO_3)_2(L)_2]$) concentrations, and plotted as a function of solute concentration. Quoted errors for these second-order rate coefficients are a combination of measurement precision and sample concentration errors.

Pulsed electron dosimetry was determined using N_2O (UHP, Air Gas) saturated, aqueous solutions of 10 mM KSCN at λ_{max} = 470 nm ($G\varepsilon = 5.2 \times 10^{-4}$ m^2 J^{-1}).[41]

Computations

Electronic structure calculations, using the Gaussian16 and Gaussview6 programs,[42,43] were employed to evaluate the energetic feasibility of discussed reactions of ligands. All geometries and energies were determined using density functional theory (DFT) with the B3LYP functional, 6-31+G(d) basis set, and Grimme *et al.*'s empirical D3 corrections for dispersion effects.[44] Solvation was included in all calculations using the polarizable continuum model for *n*-dodecane. Reaction free energies were determined using corrections for standard states.[45,46]

Density-based quantum chemical calculations were performed to understand potential differences for the binding of TBP, DEHBA, and DEH*i*BA ligands to UO_2^{2+}. We selected the dominant bis-chelate $[UO_2(NO_3)_2(ligand)_2]$ complex to investigate for our ligand and UO_2^{2+} concentration regime.[47,48] The free ligands and their corresponding UO_2^{2+} complexes in their neutral and radical cation states were studied. The density functional theory (DFT) approach as implemented in the ADF engine within the AMS2021 suite was used for this purpose.[49] Geometry optimizations were performed using the generalized gradient approximation (GGA) functional, PBE, with the STO-TZP basis set. The implicit solvent model CPCM was used to simulate the dodecane environment (ε = 2). Once the geometries were optimized and confirmed to be local minima, the final Kohn-Sham (KS) orbital sets were obtained through single point calculations using the hybrid functional, PBE0, with the STO-TZP basis set. Scalar relativistic effects for all calculations in ADF were considered using the ZORA Hamiltonian. After testing the inclusion of dispersion corrections on $[UO_2(NO_3)_2(TBP)_2]$, these effects were not considered further as they did not alter the chemical properties of these particular systems. The KS orbitals were then localized through the natural bond orbital (NBO) analysis as implemented in AMS2021.[50,51] The natural localized molecular orbitals (NLMOs) and its relevance in chemistry have been highlighted elsewhere.[52]

The global and local chemical reactivity of the free and complexed ligands have been investigated by means of the global Fukui function for electrophilic reaction (**Equation 7**),[53] and its condensed variant (**Equation 8**),[54] respectively.

$$f^- = p(N) - p(N-1), \quad (7)$$

$$f_k^- = q_N(N) - q_N(N-1). \quad (8)$$

Here, 'N' refers to the neutral species and 'N–1' to the radical cation. Thus, f^- is related to changes in the molecular density upon the removal one electron (in the frozen density approximation),[55] while f_k^- allows identification of reactive centers through variations in the atomic charges. For the latter the Mülliken charges were considered. In addition to the Fukui functions, the local softness (s_k^-) was also calculated from the global softness (S) according to the following equations,

$$S = \frac{1}{ELUMO - EHOMO}, \quad (9)$$

$$s_k^-(r) = S f_k^-(r). \quad (10)$$

These calculations were also performed in the AMS2021 suite.

Results and Discussion

Although all three ligands have been shown to form higher order structures under high ligand concentration conditions in the presence and absence of metal ions,[22-26] the relatively dilute solution conditions used here for kinetic measurements guarantee that the presented data reflects the behaviour of predominantly monomeric ligand systems and bis-chelate UO_2^{2+} complexes only.

TBP. Radiation chemical reaction kinetics for $RH^{\bullet+}$ with free TBP are shown in **Figure 2**. Despite the prevalence of TBP in reprocessing technology, the second-order rate coefficient (*k*) for the reaction of $RH^{\bullet+}$ with free TBP has not been previously measured, and yet it is an essential value for the development of predictive computer models for ligand radiolysis under reprocessing conditions.

The raw kinetic data obtained at 800 nm for $RH^{\bullet+}$ reaction with free TBP in 0.5 M DCM/*n*-dodecane solution is shown in **Figure 2A**. These decays are seen to become faster at higher ligand concentrations. The data were individually fitted to a general, double-exponential, decay function:

$$k_{obs} = A_1 exp^{-k_1 t} + A_2 exp^{-k_2 t} + B, \quad (11)$$

giving the solid curves shown. Longer time measurements (> 100 ns) showed that this transient absorption completely decayed back to baseline, and hence the baseline adjustment parameter (*B*) was set to zero in all fittings. It is also important to note that the initial starting point for these fittings was carefully checked to ensure that the system rise-time (estimated at ca. 1 ns) did not distort the calculated values. Slightly different pseudo-first-order rate coefficients (*k'*) were obtained when the fitting was begun at the peak intensity. However, the fitted parameters obtained using the first point after signal peak (as shown in **Figure 2A**) were consistent with data calculated for later starting times, and hence these were used. Single-exponential decay fitting to these data was also attempted, but it was found that the latter part of the decay was not well fitted using only this reduced function. This is a consequence of $RH^{\bullet+}$ decay in the absence of solutes being composed of two components: *(i)* ultra-fast geminate cation-electron ($^1e^-$) recombination and *(ii)* non-geminate or homogenous cation-electron ($^2e^-$) recombination, **Equations 12** and **13**, respectively:

$$^1RH^{\bullet+} + {}^1e^- \rightarrow RH^*, \quad (12)$$

$$^1RH^{\bullet+} + {}^2e^- / {}^2RH^{\bullet+} + {}^1e^- \rightarrow RH^*. \quad (13)$$

The non-geminate electrons are quantitatively scavenged by the 0.5 M DCM present in our solutions. Further, at the time point of fitting these data (~2-3 ns), a substantial fraction of geminate recombination is complete due to the low polarity of the medium and the high mobility of the solvated electron. Thus, the observed decay of $RH^{\bullet+}$ in the presence of TBP mostly reflects the homogeneous $RH^{\bullet+}$ reaction with TBP (k_1). At longer times there is a slower decay in wavelength (k_2), which is not dependent upon the solute concentration. To account for both decays, a double-exponential, decay function was used. The calculated pseudo-first-order rate coefficients from the first (k_1) component of the double-exponential fit ranged from (3-5) × 10^8 s^{-1}, these are plotted against TBP concentration, as shown in **Figure 2B**. A weighted linear fit to these data gives the second-order rate coefficient (*k*) for this reaction, the value for TBP being $k(RH^{\bullet+} + TBP) = (1.3 \pm 0.1) \times 10^{10}$ M^{-1} s^{-1}. This rate coefficient is ~30% faster than the second-order rate coefficient previously reported for free DEHBA, $k(RH^{\bullet+} + DEHBA) = (1.04 \pm 0.02) \times 10^{10}$ M^{-1} s^{-1},[13] but slower than the rate reported for DEH*i*BA ($(1.52 \pm 0.11) \times 10^{10}$ M^{-1} s^{-1}).[14]

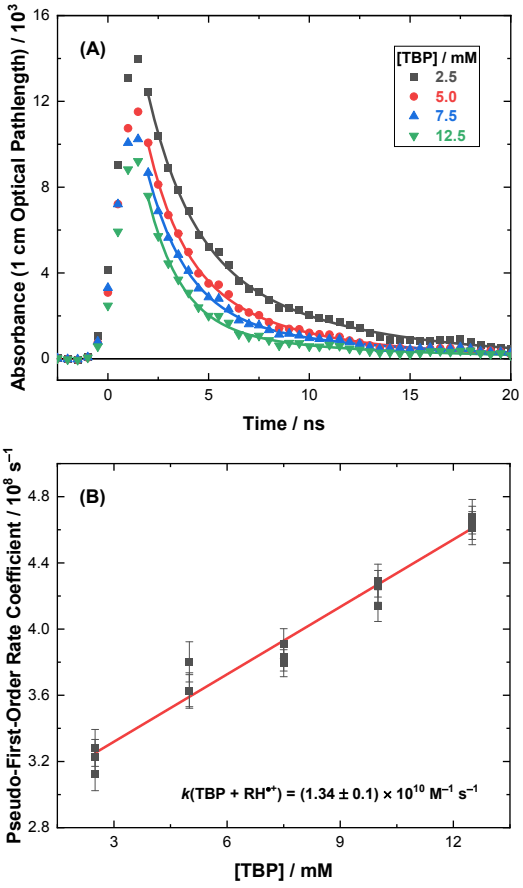

Fig. 2. (**A**) Double-exponential fitting for $RH^{\bullet+}$ decays at 800 nm with free TBP in 0.5 M DCM/*n*-dodecane solution. (**B**) Second-order determination of the rate coefficient (*k*) for the reaction of $RH^{\bullet+}$ with free TBP in 0.5 M DCM/*n*-dodecane solution at 800 nm. Solid line corresponds to a weighted linear fit, with slope equal to the second-order rate coefficient: $k(RH^{\bullet+} + TBP) = (1.3 \pm 0.1) \times 10^{10}$ M^{-1} s^{-1}, $R^2 = 0.96$.

Complexation of UO_2^{2+} by TBP affords a dimeric complex, $[UO_2(NO_3)_2(TBP)_2]$, under the dilute conditions used here. Measurement of the corresponding $RH^{\bullet+}$ reaction was achieved by varying the UO_2^{2+} concentration from 0.67-5.4 mM, and always keeping the TBP concentration a factor of 5.5 × higher. While both species concentrations varied, albeit their ratio was constant, it was assumed that the $[UO_2(TBP)_2(NO_3)_2]$ complex was always fully formed under these conditions. The free concentration of TBP was calculated by mass balance, and by subtraction of its associated kinetic component using the free ligand measured rate coefficient, allowing the magnitude of the complexes' rate coefficient to be readily determined. However, the presence of UO_2^{2+} was found to not impact the overall reactivity of $RH^{\bullet+}$ with TBP under these conditions, in contrast

to previously metal-coordinated ligand systems, i.e., HONTA and HEH[EHP].[28,29]

$[UO_2(NO_3)_2(DEHBA)_2]$ and $[UO_2(NO_3)_2(DEHiBA)_2]$. Kinetics for the reaction of $RH^{\bullet+}$ with UO_2^{2+} complexes of DEHBA ($[UO_2(NO_3)_2(DEHBA)_2]$) and DEH*i*BA ($[UO_2(NO_3)_2(DEHiBA)_2]$) are shown in **Figures 3A** and **3B**, respectively. The raw kinetic data for these figures is provided in the Supplementary Information (SI), **Figures S1** and **S2**. These kinetic data were obtained as for TBP above, by using a fixed ratio of ligand to UO_2^{2+} (DEHBA, 6.2x and DEHiBA, 7.53x) in solution and assuming that the full complex was always formed. Both ligands exhibited a large increase in their rate of reaction with $RH^{\bullet+}$ upon complexation with UO_2^{2+}. For $[UO_2(NO_3)_2(DEHBA)_2]$, a second-order rate coefficient of (2.5 ± 0.1) × 10^{10} M^{-1} s^{-1} was derived from the fitted pseudo-first order decays using a free DEHBA value of k = 9.3 × 10^9 M^{-1} s^{-1} (~10% lower than that previously reported).[13] This slightly lower value for the free ligand was due to re-analysis of these free DEHBA data, now using the same fitting procedure as described above for free TBP. In addition, the previously reported rate coefficients for free DEHBA ((1.04 ± 0.02) × 10^{10} M^{-1} s^{-1})[13] and DEH*i*BA ((1.59 ± 0.08) × 10^{10} M^{-1} s^{-1})[14] had used much higher concentrations of these ligands (10 - 40 mM) and fitting of these data to a double-exponential decay function gave pseudo-first-order rate coefficients close to 1 × 10^9 s^{-1}, which could have been considerably distorted by the system rise-time (estimated at ca. 1 ns). Hence re-analysis of these kinetic data was performed with any fitted pseudo-first-order rate coefficients above 6 × 10^8 s^{-1} not included. This resulted in better linear second-order fits, and a slight rate coefficient decrease for DEHBA (k = (9.3 ± 0.02) × 10^9 M^{-1} s^{-1}). This was important, as the $[UO_2(NO_3)_2(L)_2]$ rate coefficients are very dependent upon the accurate subtraction of the dominant free ligand reaction component. Correspondingly, a corrected rate coefficient for DEH*i*BA of k = (1.1 ± 0.04) × 10^{10} M^{-1} s^{-1} (~25% lower than previously reported)[14] was also calculated. Subtracting the contributions of these corrected rate coefficients, it was seen that the $[UO_2(NO_3)_2(DEHBA)_2]$ was over double (2.67×) the free ligand value while for $[UO_2(NO_3)_2(DEHiBA)_2]$, a second-order rate coefficient of (1.6 ± 0.1) × 10^{10} M^{-1} s^{-1} was derived, affording a 39% increase in rate in comparison to the free ligand under these conditions.

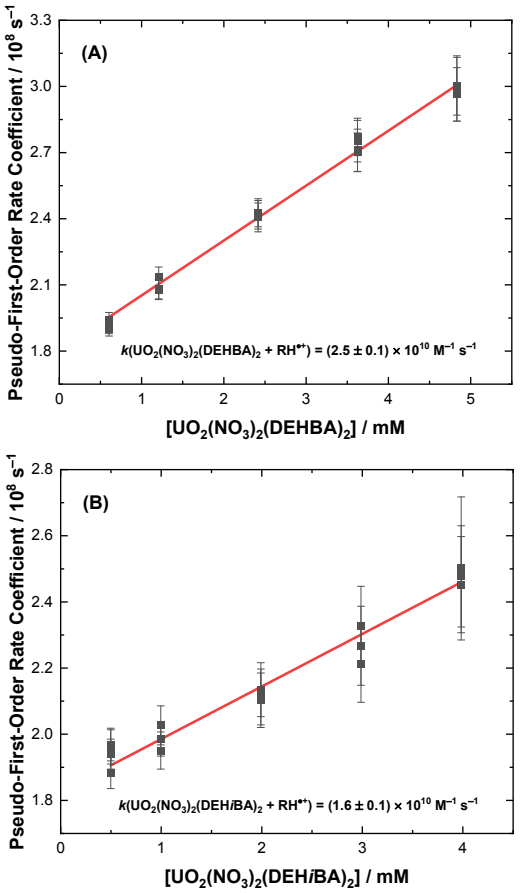

Fig. 3. Second-order determination of the rate coefficients (k) for the reaction of $RH^{\bullet+}$ with $[UO_2(NO_3)_2(DEHBA)_2]$ **(A)** and $[UO_2(NO_3)_2(DEHiBA)_2]$ **(B)** in 0.5 M DCM/*n*-dodecane solution at 800 nm. Solid lines correspond to a weighted linear fit, with slope equal to the second-order rate coefficient: $k(RH^{\bullet+} + [UO_2(NO_3)_2(DEHBA)_2])$ = (2.5 ± 0.1) × 10^{10} M^{-1} s^{-1} and $k(RH^{\bullet+} + [UO_2(NO_3)_2(DEHiBA)_2])$ = (1.6 ± 0.1) × 10^{10} M^{-1} s^{-1}, R^2 = 0.99 and 0.96, respectively.

Discussion

The presence or absence of a $RH^{\bullet+}$ reaction rate enhancement upon UO_2^{2+} complexation between the investigated ligands suggests differences in reaction mechanism and distribution of electron density upon complexation.

With regards to differences in radiolytic mechanism, the interaction of $RH^{\bullet+}$ with a ligand can proceed via one of two possible reaction pathways, electron/hole transfer (**Equation 14**) or proton transfer (**Equation 15**):

$$RH^{\bullet+} + Ligand \rightarrow RH + [Ligand]^{\bullet+}, \quad (14)$$

$$RH^{\bullet+} + Ligand \rightarrow R^{\bullet} + [Ligand(+H)]^{+}. \quad (15)$$

Electron/hole transfer only occurs if energetically feasible – often evaluated by comparing the ionization potentials (IP) of the ligand *vs.* the solvent. Because these are not available, computed values in the *n*-dodecane solvent were used, in this case *n*-dodecane IP = 8.14 eV and IP = 8.36 eV for TBP, indicating the electron/hole transfer process is energetically unfavourable. With correction for standard states, a reaction free energy (ΔG) of 0.16 eV was determined. By contrast, in similar computations, proton transfer is found to be favourable, with ΔG = -0.36 eV. Whereas, either $RH^{\bullet+}$ reaction pathway is energetically favourable for the butyramides (DEHBA and DEH*i*BA IPs = 7.20 and 7.18 eV in *n*-dodecane), although electron/hole transfer has a greater negative free energy, as shown in **Table 1**.

Table 1. Electronic structure calculation free energy (ΔG) values for the reaction of $RH^{\bullet+}$ with TBP, DEHBA, and DEH*i*BA for electron/hole transfer and proton transfer scenarios.

Ligand	$\Delta G_{electron/hole\ transfer}$ (eV)	$\Delta G_{proton\ transfer}$ (eV)
TBP	0.16	-0.36
DEHBA	-0.88	-0.60
DEH*i*BA	-0.90	-0.57

We note that the conclusions drawn from the computational results in **Table 1** did not change with different methods or whether dispersion was included or not, see SI **Table S1**. Another reason electron/hole transfer likely dominates is that it can occur at a larger distance than proton transfer, as the reactants diffuse together. These calculations indicate that part of the reason for absence of kinetic enhancement for the reaction of $RH^{\bullet+}$ with TBP is due to a fundamental difference in reaction mechanism, i.e., proton transfer, which is not amenable to the inner-sphere effects of complexation.

However, electronic and structural effects upon UO_2^{2+} complexation with these ligands also plays a role. The Fukui function has been widely utilized to predict the regions in a molecule that are susceptible to a nucleophilic/electrophilic reaction.[53,54] Herein, we rely on the global (f^-) and local (f_k^-) Fukui functions to elucidate the differences in reactivity of the free and complexed ligand systems upon electrophilic attack by $RH^{\bullet+}$. For this purpose, in addition to the three free ligands, the bis-chelate uranyl complexes, $[UO_2(NO_3)_2(L)_2]$, and their corresponding radical cation counterparts ($L^{\bullet+}$ and $[UO_2(NO_3)_2(L)_2]^{\bullet+}$, respectively) were calculated.

A first insight into reactivity can be obtained by inspecting the bond lengths of the geometry-optimized systems (**SI Table S2-S4**). Two comparisons are useful for this purpose, the structural differences between neutral and radical species, and between free and complexed ligands. For TBP, it is clear that the phosphate P=O double bond distance is increased in the radical cation ($TBP^{\bullet+}$) compared to the neutral species. This implies that the electron hole would involve the electron density of the double bond. This distance is also increased when TBP complexes UO_2^{2+} due to forward donation of electron density to the metal center. This distance is further elongated when the radical is formed in the complex, but not more than the elongation of the U–NO_3^- bonds (**SI Table S2**). A different picture is seen in the DEHBA and DEH*i*BA calculations; their amide C=O bonds contract at the expense of the amide C–N bond when moving from the neutral to the radical cation species (**SI Table S3-S4**). The same trend is observed upon butyramide complexation, implying that coordination does not change the structure of the free amide ligands to any significant extent. In addition, elongation of the U–DEHBA/DEH*i*BA bond was observed in the radical cation form compared to the neutral species.

A qualitative insight can also be obtained by inspection of the molecular orbitals of the $L^{\bullet+}$ and its corresponding UO_2^{2+} complex, particularly comparing the hole created by the removal of one electron by $RH^{\bullet+}$. Interestingly, the electron hole on TBP spreads out from the oxygen atoms toward the alkyl chains, in contrast to $[UO_2(NO_3)_2(TBP)_2]^{\bullet+}$ where the hole mostly localizes on the complexed NO_3^- ligands (**Figure 4**). A similar picture to that of free $TBP^{\bullet+}$ is observed for free $DEHBA^{\bullet+}$ and $DEHiBA^{\bullet+}$, where the hole spreads out from the amide group to the alkyl chains. However, unlike $TBP^{\bullet+}$, this effect is extended to the corresponding butyramide UO_2^{2+} complexes, which presents a critical difference between the phosphate- and the amide-based ligands. The neutral species provide further support to this difference, the free TBP ligand has its highest occupied molecular orbitals (HOMOs) localized on the phosphate moiety, whereas $[UO_2(NO_3)_2(TBP)_2]$ has its two first HOMOs localized on the attendant NO_3^- ligands (**SI Figure S3**). Conversely, $[UO_2(NO_3)_2(DEHBA)_2]$ (**SI Figure S4**) and $[UO_2(NO_3)_2(DEHiBA)_2]$ (**SI Figure S5**) complexes have their two first HOMOs predominantly localized on the amide moieties, suggesting that the oxidation of: *(i)* $[UO_2(NO_3)_2(TBP)_2]$ would most likely occur on one of the complexed NO_3^- ligands, which is in agreement with the calculated energetic unfavorability of the $RH^{\bullet+}$ electron/hole transfer with TBP, **Table 1**; and (ii) $[UO_2(NO_3)_2(DEHBA)_2]$/$[UO_2(NO_3)_2(DEHiBA)_2]$ reaction would occur at one of the coordinated DEHBA/DEH*i*BA molecules, further supporting the calculated energetic favourability of these ligands towards electron/hole transfer with $RH^{\bullet+}$, **Table 1**.

The picture given by the MO inspection is further confirmed by the plots of global electrophilic Fukui function f^- (**Figure 4**). Again, when TBP is complexed to UO_2^{2+}, the attendant NO_3^- ligands 'shield' the TBP molecules from electrophilic attack by $RH^{\bullet+}$. This is not the case for DEHBA/DEH*i*BA, where the presence of complexed NO_3^- ligands does not protect them due to the reactivity of the amide group. To further develop this description, the wavefunctions of DEHBA, DEH*i*BA, and their UO_2^{2+} derivatives were localized through the natural bond orbital (NBO) approximation. The NBO analysis identified an electron deficient 3-center 4-electron bond (hyperbond) formed by the N-atom lone pair and the C=O double bond that is not present in TBP. The localization of the N-lone pair and the C=O double bond dominates the resonant structures (64%). This is changed when these ligands are complexed to UO_2^{2+}, where the two resonant structures are equally weighted, implying that the coordination of DEHBA/DEH*i*BA allows the amide N-atom to delocalize its density toward the amide O atom.

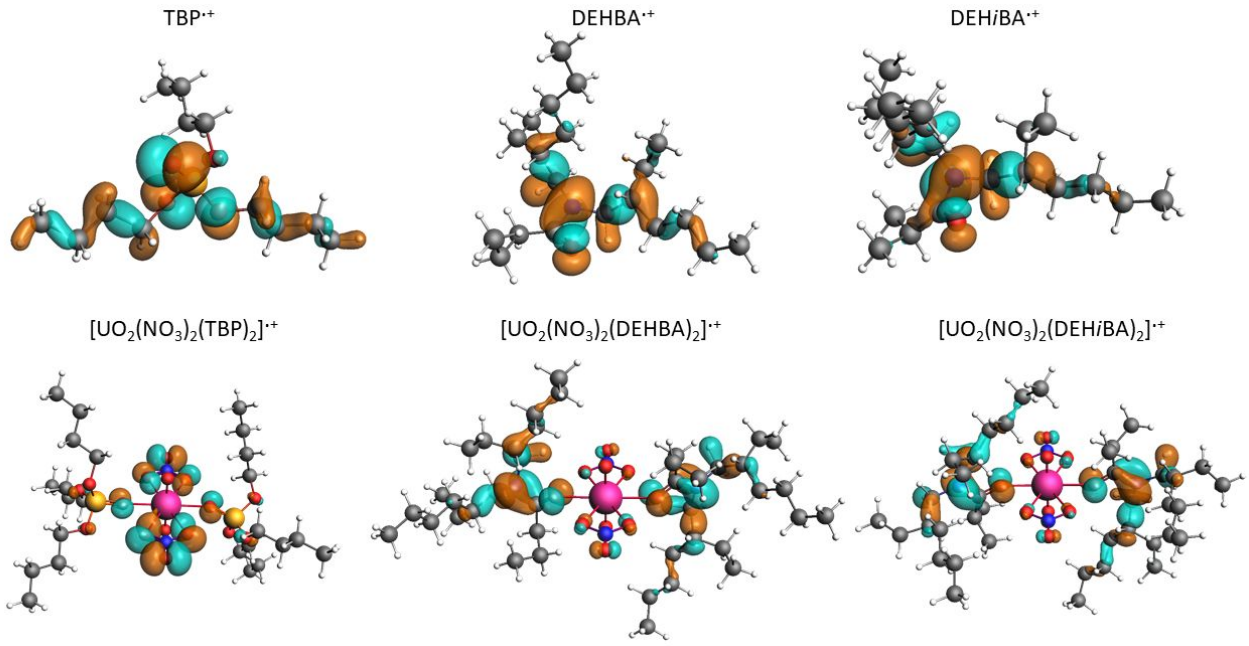

Fig. 4. Canonical Kohn-Sham molecular orbitals of the electron holes in the geometry-optimized radical cation species.

The condensed electrophilic Fukui functions f_k^- were obtained to further identify the most reactive centers in the molecules and complexes. Consistently with the other analyses, it is predicted that in TBP, the centers most susceptible to electrophilic attack are the O-atoms (f_k^- = 0.093 – 0.136) with the O-atom where the double bond is localized displaying the largest value (**SI Table S5**). The scenario changes completely upon UO_2^{2+} complexation, where the reactivity of these centers is totally decreased, and only present on the non-coordinating O-atoms of the attendant NO_3^- ligands, reaching a similar magnitude to that of phosphate O-atoms for free TBP. The same conclusion is observed by analysing the softness of these centers (**SI Table S5**). Interestingly, more details are obtained regarding the amide ligands, while the carbonyl O-atom in DEHBA and DEH*i*BA is predicted to be the most reactive center, the amide N-atom is found to be most reactive in their corresponding UO_2^{2+} complexes. A slight difference in the softness of the centers is observed in the DEH*i*BA systems, where unlike DEHBA, the correspondence between the Fukui function and local softness deviates for the free ligand, i.e., the amide O-atom is the most reactive but not the softest center, though this is more anecdotal than a reason for expecting changes in reactivity.

Finally, the uranyl-ligand (U–L) interaction was interrogated by means of the natural localized molecular orbitals (NLMOs), which provide a more realistic picture of the chemical interaction than that of the canonical molecular orbitals.[52] **SI Table S8** shows the main U–L interactions including the oxo ligands for comparison. Here, as expected the U–L bonds are rather weak compared to the axial oxo ligands, with 22% ($U–O_{yl}$) versus 4-8% ($U–O_L$) of metal contribution to the NLMO. It is important to bear in mind that the actinide-ligand interactions are considered either mostly ionic or highly polar covalent, which means that the metal contribution to the bond is not expected to be as high as 50%. Between TBP, DEHBA, and DEH*i*BA, the latter two display the strongest U–L bonds, where the interaction is dominated by a σ-type NLMOs with 8% U contribution. On the other hand, TBP only shows very polarized σ-bonds NLMOs with only 4% of metal orbital mixing. This bonding picture correlates with the effect of complexation on the change of the intrinsic nature of the hyperbond in DEHBA and DEH*i*BA, which is not present in TBP.

Conclusions

Pulsed electron irradiation techniques have been used to measure radiation chemical kinetics for the reaction of $RH^{\bullet+}$ with TBP, DEHBA, and DEH*i*BA and their corresponding UO_2^{2+} complexes, for which a summary of determined rate coefficients is give in **Table 2**. These measurements clearly show that UO_2^{2+} complexation has: *(i)* negligible effect on the reaction of $RH^{\bullet+}$ with TBP; and *(ii)* significantly increases the rate of reaction between $RH^{\bullet+}$ and DEHBA/DEH*i*BA.

Table 2. Summary of second-order $RH^{\bullet+}$ rate coefficients measured or revised by this work for TBP, DEHBA, and DEH*i*BA in 0.5 M DCM/*n*-dodecane solutions with and without UO_2^{2+} present.

Sample	$RH^{\bullet+}$ Rate Coefficient (10^{10} M^{-1} s^{-1})	Reference
TBP	1.4 ± 0.1	*This Work*
$[UO_2(NO_3)_2(TBP)_2]$	-	*This Work*
DEHBA	0.9 ± 0.02	Revised from 13
$[UO_2(NO_3)_2(DEHBA)_2]$	2.5 ± 0.1	*This Work*
DEH*i*BA	1.1 ± 0.04	Revised from 14
$[UO_2(NO_3)_2(DEHiBA)_2]$	1.6 ± 0.1	*This Work*

The differences in kinetic enhancement between the two ligand classes is attributed to: *(i)* the energetic favourability for DEHBA/DEH*i*BA to undergo electron/hole transfer with $RH^{\bullet+}$, which is believed to extended to their corresponding UO_2^{2+} complexes owing to subtle changes in structure and electron distribution that favour the amide resonance, and thus are amenable to inner-sphere processes conferred by complexation; and *(ii)* TBP only interacts with $RH^{\bullet+}$ via proton transfer, which is not amenable to inner-sphere processes, and that the corresponding UO_2^{2+} complexes' attendant NO_3^- ligands shield the TBP molecule, as the unbonded oxygen provides a likely site for proton transfer from $RH^{\bullet+}$.

These results suggest that in the PUREX process, most of the radiolytic damage to TBP is by direct ionization or reaction with subsequent degradation product radicals, and not from oxidation by $RH^{\bullet+}$. Whereas the converse is indicated for the butyramides, which may have an impact upon their applicability as TBP substitutes. Future UO_2^{2+} loaded TBP/DEHBA/DEH*i*BA gamma irradiations are underway to determine the steady-state influence of metal complexation of ligand integrity, in addition to investigating how these bis-chelate system findings are affected by the introduction of the higher order structures (e.g.,. ligand trimers and oligomers)[23-26] anticipated under envisioned process conditions.

Conflicts of interest

There are no conflicts to declare.

Acknowledgements

This research has been funded by the US-DOE Assistant Secretary for NE, under the Material Recovery and Waste Form Development Campaign, DOE-Idaho Operations Office Contract DE-AC07-05ID14517 and DE-NE0008659 Nuclear Energy Universities Program (NEUP) grant.

The efforts of Cook and the picosecond pulsed electron irradiation experiments performed using the BNL Accelerator Center for Energy Research LEAF facility, were supported by the US-DOE Office of Basic Energy Sciences, Division of Chemical Sciences, Geosciences, and Biosciences under contract DE-SC0012704.

Notes and references

(1) Strategies and Considerations for the Back End of the Fuel Cycle, Nuclear Technology Development and Economics, NEA No. 7469, 2021.
(2) W.B. Lanham and T.C. Runion, PUREX process for plutonium and uranium recovery, ORNL-479, 1949, pp 1-11.
(3) K.L. Nash, C. Madic, J. Mathur, and J. Lacquement, The chemistry of the actinide and transactinide elements. 3rd Ed. Springer, 2006, 2622-798.
(4) G.V. Buxton, C.L. Greenstock, W.P. Helman and A.B. Ross, *J. Phys. Chem. Ref. Data*, 1988, **17**, 513-886.
(5) Y. Katsumura, in *The Chemistry of Free Radicals: N-Centered Radicals*, ed. Z. B. Alfassi, John Wiley & Sons, Inc., 1998.
(6) B.J. Mincher and S. P. Mezyk, *Radiochim. Acta*, 2009, **97(9)**, 519.
(7) B.J. Mincher, G. Modolo, and S.P. Mezyk, *Solv. Extr. Ion Exch.*, *2009*, **27**, 1-25.
(8) F.W. Lewis, L.M. Harwood, M.J. Hudson, A. Nunez, H. Galan and A.G. Espartero, *Synlett*, *2016*, **27**, 1.
(9) E. Macerata, E. Mossini, S. Scaravaggi, M. Mariani, A. Mele, W. Panzeri, N. Boubals, L. Berthon, M.-C. Charbonnel,F. Sansone, A. Arduini and A. Casnati, J. Am. Chem. Soc.,2016, 138, 7232.
(10) G.M. Gasparini and G. Grossi, *Solvent Extraction and Ion Exchange*, 1986, **4(6)**, 1233.
(11) K. McCann, J.A. Drader, and J.C. Braley, *Separation & Purification Reviews,* 2018, **47(1)**, 49.
(12) D.R., Prabhu, G.R. Mahajan, and G.M. Nair, *J. Radioanal. Nucl. Chem.*, *1997*, **224**, 113.
(13) G.P. Horne, C.A. Zarzana, T.S. Grimes, C. Rae, J. Ceder, S.P. Mezyk, B.J. Mincher, M.-C. Charbonnel, P. Guilbaud, G. Saint-Louis, and L. Berthon, *Dalton Trans.*, *2019*, **48**, 14450.
(14) J. Drader, G. Saint-Louis, J.M. Muller, M.-C. Charbonnel, P. Guilbaud, L. Berthon, K.M. Roscioli-Johnson, C.A. Zarzana, C. Rae, G.S. Groenewold, B.J. Mincher, S.P. Mezyk, K. McCann, S.G. Boyes, and J. Braley, *Solv. Extr. Ion Exch.*, *2017*, **35(7)**, 480.
(15) V.M. Adamov, V.I. Andreev, B.N. Belyaev, R.I. Lyubtsev, G.S. Markov, M.S. Polyakov, A.E. Ritari, and A.Y. Shil'nikov, *Soviet Radiochemistry (English Translation)*, *1988*, **29(6)**, 775.
(16) P.B. Ruikar, M.S. Nagar, and M.S. Subramanian, *J. Radioanal. Nucl. Chem.*, *1993*, **176(2)**, 103.
(17) P.B. Ruikar, M.S. Nagar, M.S. Subramanian, K.K. Gupta, N. Varadarajan, and R.K. Singh, *J. Radioanal. Nucl. Chem.*, *1995*, **196**, 171.
(18) P.B. Ruikar, M.S. Nagar, M.S. Subramanian, K.K. Gupta, N. Varadarajan, and R.K. Singh, *J. Radioanal. Nucl. Chem.*, *1995*, **201(2)**, 125.
(19) C. Musikas, *Inorganica Chimica Acta*, *1987*, **140**, 197.
(20) C. Musikas, *Sep. Sci. Tech.*, *1988*, **23(12-13)**, 1211.
(21) L. Berthon and M.-C. Charbonnel, *Ion Exch. Solv. Extr.*, *A Series of Advances*, *2010*, **19**, 429.
(22) B. Ruikar, M.S. Nagar, and M.S. Subramanian, *J. Radioanal. Nucl. Chem.*, *1992*, **159**, 167.
(23) F. Rodrigues, G. Ferru, L. Berthon, N. Boubals, P. Guilbaud, C. Sorel, O. Diat, P. Bauduin, J.P. Simonin, J.P. Morel, N. Morel-

Desrosiers, M.-C. Charbonnel, *Mol. Phys.*, *2014*, **112**, 1362.
(24) G. Ferru, D. Gomes Rodrigues, L. Berthon, O. Diat, P. Bauduin, and P. Guilbaud, *Angew. Chem.*, *2014*, **53**, 5346.
(25) P. Guilbaud, L. Berthon, W. Louisfrema, O. Diat, and N. Zorz, *Chem. Eur. J.*, *2017*, **23**, 16660.
(26) A. Paquet, O. Diat, L. Berthon, and P. Guilbaud, *J. Mol. Liq.*, *2019*, **277**, 22.
(27) G.V. Buxton and R.M. Sellers, *Coord. Chem. Rev.*, *1977*, **22(3)**, 195.
(28) T. Toigawa, D.R. Peterman, D.S. Meeker, T.S. Grimes, P.R. Zalupski, S.P. Mezyk, A.R. Cook, S. Yamashita, Y. Kumagai, T. Matsumura, and G.P. Horne, *PCCP*, *2021*, **23**, 1343.
(29) M. Baxter, C.D. Pilgrim, C. Celis Barros, D.S. Meeker, T.S. Grimes, P.R. Zalupski, C. Rae, C.A. Zarzana, S.P. Mezyk, A.R. Cook, and G.P. Horne, *Inorg. Chem.*, *2021*, in preparation.
(30) C. Zarzana, D. Peterman, G. Groenewold, L. Olson, R. McDowell, W. Bauer, and S. Morgan, *Sep. Sci. Technol.*, *2015*, **50**, 2836.
(31) D. Peterman, C. Zarzana, R. Tillotson, R. McDowell, C. Rae, G. Groenewold, and J. Law, *J. Radioanal. Nucl. Chem.*, *2018*, **316**, 855.
(32) C.A. Zarzana, G.S. Groenewold, B.J. Mincher, S.P. Mezyk, A. Wilden, H. Schmidt, G. Modolo, J.F. Wishart, and A.R. Cook, *Solv. Extr. Ion Exch.*, *2015*, **33(5)**, 431.
(33) S.P. Mezyk, B.J. Mincher, S.B. Dhiman, B. Layne and J.F. Wishart, *J. Radioanal. Nucl. Chem.*, *2016*, **307(3)**, 2445.
(34) S.P. Mezyk, G.P. Horne, B.J. Mincher, P.R. Zalupski, A.R. Cook, and J.F. Wishart, *Proc. Chem.*, *2016*, **21**, 61.
(35) J. Drader, G. Saint-Louis, J.M. Muller, M.-C. Charbonnel, P. Guilbaud, L. Berthon, K.M. Roscioli-Johnson, C.A. Zarzana, C. Rae, G.S. Groenewold, B.J. Mincher, S.P. Mezyk, K. McCann, S.G. Boyes and J. Braley, *Solv. Extr. Ion Exch.*, *2017*, **35(7)**, 480.
(36) G.P. Horne, C.A. Zarzana, T.S. Grimes, C. Rae, J. Ceder, S.P. Mezyk, B.J. Mincher, M.-C. Charbonnel, P. Guilbaud, G. Saint-Louis, and L. Berthon, *Dalton Trans.*, *2019*, **48**, 14450.
(37) P.N. Pathak, D.R. Prabhu, A.S. Kanekar, and V.K. Manchanda, *Sep. Sci. Tech.*, *2009*, **44(15)**, 3650.
(38) J.F. Wishart, A.R. Cook, and J.R. Miller, *Rev. Sci. Instr.*, *2004*, **75(11)**, 4359.
(39) S.Tagawa, N. Hayashi, Y. Yoshida, M. Washio, and Y. Tabata, *Int. J. Rad. App. Instr. C: Rad. Phys. Chem.*, *1989*, **34 (4)**, 503.
(40) Y. Yoshida, T. Ueda, T. Kobayashi, H. Shibata, S. Tagawa, *Nuclear Instruments and Methods in Physics Research Section A: Accelerators, Spectrometers, Detectors and Associated Equipment*, *1993*, **327 (1)**, 41.
(41) G.V. Buxton and C.R. Stuart, *J. Chem. Soc. Faraday Trans.*, 1995, **92(2)**, 279.
(42) M.J. Frisch, G.W. Trucks, H.B. Schlegel, G.E. Scuseria, M.A. Robb, J.R. Cheeseman, G. Scalmani, V. Barone, G.A. Petersson, H. Nakatsuji, X. Li, M. Caricato, A.V. Marenich, J. Bloino, B.G. Janesko, R. Gomperts, B. Mennucci, H.P. Hratchian, J.V. Ortiz, A.F. Izmaylov, J.L. Sonnenberg, D. Williams-Young, F. Ding, F. Lipparini, F. Egidi, J. Goings, B. Peng, A. Petrone, T. Henderson, D. Ranasinghe, V.G. Zakrzewski, J. Gao, N. Rega, G. Zheng, W. Liang, M. Hada, M. Ehara, K. Toyota, R. Fukuda, J. Hasegawa, M. Ishida, T. Nakajima, Y. Honda, O. Kitao, H. Nakai, T. Vreven, K. Throssell, J.A. Montgomery, J.E. Peralta, F. Ogliaro, M.J. Bearpark, J.J. Heyd, E.N. Brothers, K.N. Kudin, V.N. Staroverov, T.A. Keith, R. Kobayashi, J. Normand, K. Raghavachari, A.P. Rendell, J.C. Burant, S.S. Iyengar, J. Tomasi, M. Cossi, J.M. Millam, M. Klene, C. Adamo, R. Cammi, J.W. Ochterski, R.L. Martin, K. Morokuma, O. Farkas, J.B. Foresman, and D.J. Fox, Gaussian 16, Revision A.03. Gaussian, Inc., Wallingford CT, 2016.
(43) R. Dennington, T. Keith, and J. Millam, GaussView, Version 6.1.1. Semichem Inc., Shawnee Mission, KS, 2019.
(44) S. Grimme, J. Antony, S. Ehrlich, and H. Krieg, *J. Chem. Phys.*, *2010*, **132**, 154104.
(45) C.P. Kelly, C.J. Cramer, and D.G. Truhlar, *J. Phys. Chem. B*, *2006*, **110(32)**, 16066.
(46) C.P. Kelly, C.J. Cramer, and D.G. Truhlar, *J. Phys. Chem. B*, *2007*, **111(2)**, 408.
(47) G. Benay and G. Wipff, *J. Phys. Chem. B*, *2014*, **118(11)**, 3133.
(48) P. Sahu, S.M. Ali, K.T. Shenoy, *Phys. Chem. Chem. Phys.*, *2016*, **18(34)**, 23769.
(49) ADF 2021.1, SCM, Theoretical Chemistry, Vrije Universiteit, Amsterdam, The Netherlands, http://www.scm.com.
(50) E.D. Glendening, J.K. Badenhoop, A.E. Reed, J.E. Carpenter, J.A. Bohmann, C.M. Morales, C.R. Landis, and F. Weinhold, NBO 6.0., http://nbo6.chem.wisc.edu/.
(51) E.D. Glendening, C.R. Landis, and F. Weinhold, *J. Comput. Chem.*, *2013*, **34(16)**, 1429.
(52) A.E. Reed and F. Weinhold, *J. Chem. Phys.*, *1985*, **83 (4)**, 1736.
(53) P.W. Ayers, and R.G. Parr, *J. Am. Chem. Soc.*, *2000*, **122(9)**, 2010.
(54) P. Fuentealba, P. Pérez, and R. Contreras, *J. Chem. Phys.*, *2000*, **113(7)**, 2544.
(55) W. Yang, R.G. Parr, and R. Pucci, *J. Chem. Phys.*, *1984*, **81(6)**, 2862.